Entropy production and irreversibility of dissipative trajectories in electric circuits

K.-H. Chiang, C.-L. Lee, P.-Y. Lai, and Y.-F. Chen*
Department of Physics, National Central University, Zhongli 32001, Taiwan
(Received 8 September 2016; revised manuscript received 10 January 2017; published 30 January 2017)

We experimentally examine the equivalence between the entropy production evaluated from irreversibility of trajectories and the physical dissipation in dissipative processes via electric resistor-capacitor (*RC*) circuits. The examinations are performed for two nonequilibrium steady states that are driven by an injected current and temperature difference, respectively. Such an equivalence demonstrates a parameter-free method to evaluate the entropy production of a system. The effects of configurational and temporal resolutions are also studied.

DOI: 10.1103/PhysRevE.95.012158

I. INTRODUCTION

The message "entropy reads the arrow of time," as stated by the second law of thermodynamics, points out the macroscopic irreversibility in dissipative processes. While the statement applies to the average behavior of macroscopic systems, occurrences of reverse configurational trajectories can still be allowed in dissipative processes and have been observed over short time intervals in systems with few degrees of freedom [1,2]. The reverse trajectories, along with their negative entropy production, can be well described under the scope of the fluctuation theorem (FT) [3–6], which has been verified experimentally in many small systems via trajectory analysis [1,7–10].

The irreversibility of a trajectory $x(t)$ is itself a measure of dissipation. In thermal equilibrium and nonequilibrium steady states (NESS), stochastic thermodynamics predicts the equivalence between the irreversibility of a trajectory and the dissipation absorbed by the reservoir(s) [11–13], i.e., $\Delta S_{\rm traj} \equiv k_B \ln \frac{P_F[x(t)|x_0]}{P_R[\tilde{x}(t)|\tilde{x}_0]} = \frac{Q}{T} \equiv \Delta S_Q$, where $P_F[x(t)|x_0]$ and $P_R[\tilde{x}(t)|\tilde{x}_0]$ are the conditional transition probabilities of the path $x(t)$ and its reverse path $\tilde{x}(t)$, respectively, k_B is the Boltzmann constant, and Q represents the net heat dissipating into the surrounding heat bath of temperature T along $x(t)$. Therefore, one can in principle evaluate the corresponding dissipation from the irreversibility of a particular trajectory. In practice, however, the evaluation is only possible via some coarse-graining procedure. In the pioneer works by Andrieux *et al.* [14,15], the relation was first verified experimentally in two NESS systems containing a Brownian particle and an electric *RC* circuit, respectively. The evaluation of dissipation due to irreversibility is performed according to a numerical algorithm where discrete time steps are considered and trajectories are identified within some path resolution; i.e., an observed trajectory can be identified with the preselected reference trajectory if the distance is less than a certain value.

In this work, we experimentally reexamine the equivalence between $\Delta S_{\rm traj}$ and ΔS_Q in single trajectory level using the template of electric resistor-capacitor (*RC*) circuits. The resistors in *RC* circuits are subject to thermal (Johnson-Nyquist) noises and their overdamped behaviors result from the same microscopic origins [16]. Thus the voltage signals can be described via stochastic thermodynamics. The systems are closely analogous to microscale particles experiencing Brownian motions [17], and have been explored in the determination of entropy production with incomplete information [18,19]. To study entropy production in dissipative processes, we particularly focus on the NESS cases. Two types of NESS are examined: The NESS is achieved either by a constant driving current [9] or by the coupling of two heat baths at different temperatures [20], as shown in Fig. 1. The equivalence between $\Delta S_{\rm traj}$ and ΔS_Q is reported in Sec. III through the comparison of their time series and their correlation coefficient, and in Sec. V through the examination of validity in FT.

In our current work the derivation of dissipation relies on the use of conditional entropy, as in NESS that often requires the knowledge of the steady-state distribution. Alternatively, it has been demonstrated in Ref. [21] that the entropy production can be derived without such a requirement, if the initial condition of the system is suitably chosen. Also note that concerning the derivation of dissipation via irreversibility $\Delta S_{\rm traj}$, we do not need a pre-selected trajectory as in Refs. [14,15]. Instead, we choose a coarse-graining scheme such that the measured voltage signals are sorted into bins. With this simple method, we can check about the dissipation derived from irreversibility for all observed trajectories except those whose time-reversed partners cannot be found. Our result of $\Delta S_{\rm traj}$ shows remarkable agreement compared to the physical dissipation ΔS_Q. Furthermore, in Sec. IV we also provide studies on the effects of resolutions in configuration space and time regarding the description of trajectories. Our experimental finding on the effect of time resolution is also examined and approved by a theoretical path-integral analysis.

II. EXPERIMENTAL SETUP

Figure 1 illustrates the experimental setups. First we consider a current-driven single *RC* circuit as shown in Fig. 1(a). The circuit parameter values $R = 9.20\ \mathrm{M\Omega}$ and $C = 429\ \mathrm{pF}$ are determined from the measured noise power spectrum of voltage V. The constant current source provides $I = 300\ \mathrm{fA}$ such that $\langle \dot{Q} \rangle = I^2 R \cong 200\ k_B T/\mathrm{s}$, where $T = 296\ \mathrm{K}$. Next we study a coupled *RC* circuit as illustrated in Fig. 1(b), which consists of two adjoining single *RC* circuits through a bridging capacitor C_c. The two resistors R_1 and R_2 are immersed in heat baths of temperatures $T_1 = 120\ \mathrm{K}$ and $T_2 = 296\ \mathrm{K}$ respectively, with the cold heat bath maintained in a dewar via liquid nitrogen vapor. The values of R_1, C_1, R_2, and C_2 are also resolved from the measured noise power spectra of V_1 and

*yfuchen@ncu.edu.tw

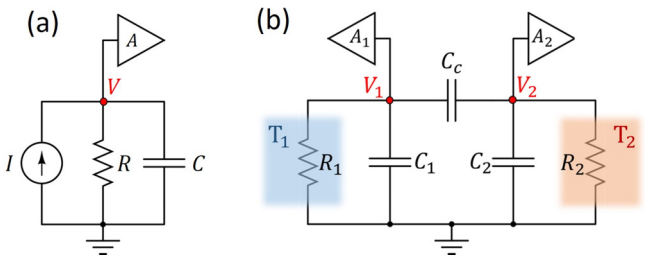

FIG. 1. Schematics of experimental setups. (a) A single *RC* circuit driven by a constant current source [9], where $I = 300\,\text{fA}$, $C = 429\,\text{pF}$, $R = 9.20\,\text{M}\Omega$. (b) A capacitively coupled *RC* circuit with two resistors kept at different temperatures [20], where $C_1 = 488\,\text{pF}$, $R_1 = 9.01\,\text{M}\Omega$, $T_1 = 120\,\text{K}$, $C_2 = 420\,\text{pF}$, $R_2 = 9.51\,\text{M}\Omega$, $T_2 = 296\,\text{K}$, and the coupling capacitor $C_c = 1.0\,\text{nF}$.

V_2 under the uncoupled condition. The low-noise amplifiers A, A_1, and A_2 are set with a voltage gain of 10^4. The circuits are shielded in a Faraday cage to avoid noise induced by electromagnetic radiations. Throughout the experiments, we record the voltage time series with a sampling rate of 2048 Hz, which corresponds to a time resolution of $\Delta t = 4.88\times10^{-4}$ s. A total number of 10^6 data are recorded during each experimental run. The experimental setups and calibrations are done similarly to those described in the pioneered works for studying FT in NESS in overdamped *RC* circuits [9,20]. (See also the Appendices for more information. The noise of the amplifiers is shown to be negligible through our study.) In the analysis of entropy production, for statistical purposes, the measured voltages are sorted into bins of width V_{bin}.

III. TEST OF EQUIVALENCE BETWEEN HEAT AND TRAJECTORY ENTROPY PRODUCTION

A. Single *RC* circuit

We first consider the NESS maintained by a constant current source [see Fig. 1(a)], using the voltage V as the observable. To facilitate the data analysis, we define a trajectory $V(t) \xrightarrow{n} V(t+\tau)$ occurring over duration τ as a discrete voltage time series, where n stands for the number of time steps and the arrow indicates the direction of time. Unless mentioned otherwise, we choose $\tau = n\Delta t$. The corresponding dissipation, or the dissipated work, is defined as the net heat flowing to the heat bath through the resistor. Thus the entropy production from heat can be computed as $\Delta S_Q^{(n)} = \sum_t^{t+\tau} V i_R \Delta t/T$, where $i_R = I - C\dot{V}$ is the current flowing through R [9]. In the meantime, one can obtain the joint probability $P[V(t) \xrightarrow{n} V(t+\tau)]$ by counting its occurrences from all measured trajectories, and the conditional transition probability $P[V(t) \xrightarrow{n} V(t+\tau)|V(t)] = P(V(t) \xrightarrow{n} V[t+\tau)]/P_{\text{ss}}[V(t)]$, where $P_{\text{ss}}(V)$ is the steady-state probability distribution.

To investigate the irreversibility of a process, we look for the occurrences of its reverse trajectory $V(t+\tau) \xrightarrow{n} V(t)$. Note that the reverse trajectory has to be found in the scenario where the NESS is maintained by a negated current source $I = -300\,\text{fA}$ [12]. Alternatively, due to the symmetry of the circuit, the same scenario can be achieved simply by negating the measured voltage time series without current inversion.

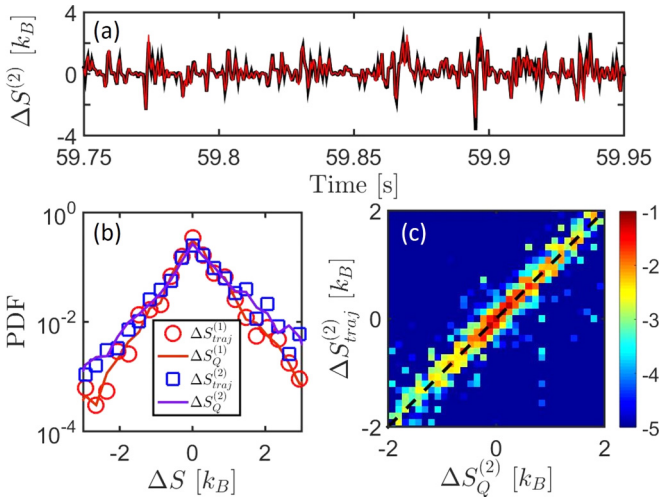

FIG. 2. Equivalence between heat and trajectory entropy production in current-driven NESS. (a) Snapshot of the time series of $\Delta S_Q^{(2)}$ (red line) and $\Delta S_{\text{traj}}^{(2)}$ (black line). (b) Probability distribution of $\Delta S_Q^{(n)}$ (solid lines) and $\Delta S_{\text{traj}}^{(n)}$ (symbols) for $n = 1$ and 2. (c) Joint probability distribution $\log P(\Delta S_Q^{(2)}, \Delta S_{\text{traj}}^{(2)})$. The black dashed line of unit slope is provided as a guide.

The trajectory entropy production of the path $V(t) \xrightarrow{n} V(t+\tau)$ is defined by

$$\Delta S_{\text{traj}}^{(n)} \equiv k_B \ln \frac{P_F[V(t) \xrightarrow{n} V(t+\tau)|V(t)]}{P_R[V(t+\tau) \xrightarrow{n} V(t)|V(t+\tau)]}, \qquad (1)$$

where $P_F[V(t) \xrightarrow{n} V(t+\tau)|V(t)]$ and $P_R[V(t+\tau) \xrightarrow{n} V(t)|V(t+\tau)]$ are the conditional forward and backward transition probabilities provided that their initial states are $V(t)$ and $V(t+\tau)$, respectively. Note that for those trajectories with large positive entropy production, their corresponding reverse trajectories have negative entropy production of the same magnitude [see Eq. (1)]. As a consequence, the occurrences of these reverse trajectories are pretty rare, and the reverse events can sometimes be even missing due to the limitation of finite observation time. For the trajectories where their reverse partners cannot be found, $\Delta S_{\text{traj}}^{(n)}$ cannot numerically be defined from the experiment (or it can be treated as positive infinity).

To directly compare $\Delta S_{\text{traj}}^{(n)}$ and $\Delta S_Q^{(n)}$ side by side for each single event, the trajectories where no reverse partners can be found are excluded from the original set of trajectories. The distributions $P(\Delta S_{\text{traj}}^{(n)})$ and $P(\Delta S_Q^{(n)})$ are derived from the new set of trajectories, while the original heat entropy production distribution $P(\Delta S_{Q0}^{(n)})$ is derived from the original set. Note that the exclusion of these events can result in systematic biases toward $P(\Delta S_{\text{traj}}^{(n)})$ and $P(\Delta S_Q^{(n)})$, since the entropy production of these events is mostly large and positive. The extent of such biases can be investigated by referring to $P(\Delta S_{Q0}^{(n)})$, as is discussed in Sec. IV.

Figure 2(a) shows a snapshot of our derived time series $\Delta S_Q^{(2)}$ (red line) and $\Delta S_{\text{traj}}^{(2)}$ (black line) using $V_{\text{bin}} = 1\,\mu\text{V}$. The two results match remarkably well, while small deviations can be observed from their probability distribution functions (PDF) as shown in Fig. 2(b) [for both 1-step ($n = 1$) and 2-step ($n = 2$) transitions]. The results of $P(\Delta S_{\text{traj}}^{(n)})$ are slightly

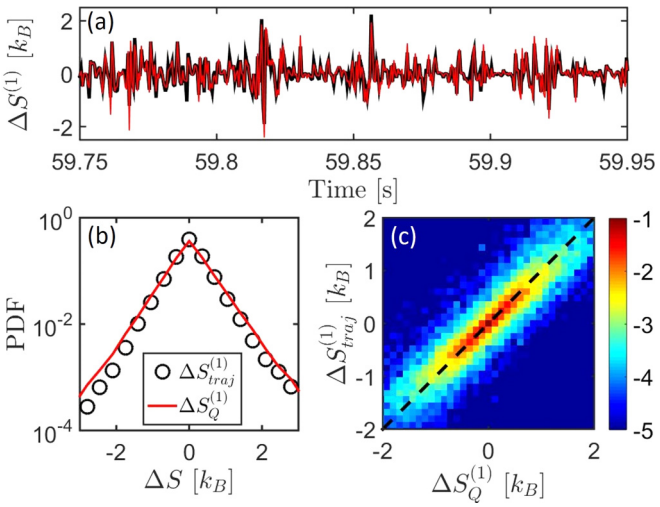

FIG. 3. Equivalence between heat and trajectory entropy production in temperature-driven NESS. (a) Snapshot of the time series of $\Delta S^{(1)}_Q$ (red line) and $\Delta S^{(1)}_{\rm traj}$ (black line) using $V_{\rm bin} = 0.5$ μV. (b) Probability distribution of single-step entropy production $\Delta S^{(1)}_Q$ (solid line) and $\Delta S^{(1)}_{\rm traj}$ (symbol). (c) Joint probability distribution $\log P(\Delta S^{(1)}_Q, \Delta S^{(1)}_{\rm traj})$. The black dashed line of unit slope is provided as a guide.

more scattered (which is more prominent in the case $n = 2$) due to the statistical uncertainties of rare events. Our results give the averages $\langle \Delta S^{(1)}_{\rm traj}\rangle = 9.57\times10^{-2}$ k_B, $\langle \Delta S^{(1)}_{Q}\rangle = 9.79\times10^{-2}$ k_B, $\langle \Delta S^{(2)}_{\rm traj}\rangle = 1.96\times10^{-1}$ k_B, and $\langle \Delta S^{(2)}_{Q}\rangle = 1.96\times10^{-1}$ k_B. As a comparison, the analytically predicted values are $\langle \Delta S^{(2)}\rangle = 2\langle \Delta S^{(1)}\rangle = 2I R^2 \Delta t/T = 1.96\times10^{-1}$ k_B. In Fig. 2(c) we present the joint probability $\log P(\Delta S^{(2)}_Q, \Delta S^{(2)}_{\rm traj})$. The correlation coefficient between $\Delta S^{(n)}_Q$ and $\Delta S^{(n)}_{\rm traj}$ is 0.97 for both $n = 1$ and $n = 2$ cases. Our experimental results provide firm evidence that the entropy evaluated from path irreversibility indeed gives the authentic entropy dissipation.

B. Temperature-driven coupled circuit

As a second example, we consider a capacitively coupled RC circuit, of which the two resistors are subject to different heat baths [see Fig. 1(b)]. Similar to the construction in the single RC case, we use $\vec{V} \equiv (V_1, V_2)$ as our experimental state observables. And the net entropy dissipation in a trajectory $\vec{V}(t) \xrightarrow{n} \vec{V}(t+\tau)$ is $\Delta S^{(n)}_Q = \sum_t^{t+\tau} (\frac{V_1 i_{R1}}{T_1} + \frac{V_2 i_{R2}}{T_2})\Delta t$, where $i_{R1} = -C_1\dot{V}_1 - C_c(\dot{V}_1 - \dot{V}_2)$ and $i_{R2} = -C_2\dot{V}_2 - C_c(\dot{V}_2 - \dot{V}_1)$ are the currents through R_1 and R_2, respectively [20]. Meanwhile, for the same process, one has $\Delta S^{(n)}_{\rm traj} = k_B \ln \frac{P_F[\vec{V}(t)\xrightarrow{n}\vec{V}(t+\tau)|\vec{V}(t)]}{P_R[\vec{V}(t+\tau)\xrightarrow{n}\vec{V}(t)|\vec{V}(t+\tau)]}$. A snapshot of the time traces and the PDF distributions for both entropies are presented in Figs. 3(a) and 3(b), respectively, for single-step transitions. Our experimental data lead to the averages $\langle \Delta S^{(1)}_{\rm traj}\rangle = 1.95\times10^{-2}$ k_B and $\langle \Delta S^{(1)}_{Q}\rangle = 1.55\times10^{-2}$ k_B. As a reference, the analytical prediction gives $\langle \Delta S^{(1)}\rangle = \langle \dot{Q}\rangle \Delta t(\frac{1}{T_1} - \frac{1}{T_2}) = 1.46\times10^{-2}$ k_B, where $\langle \dot{Q}\rangle = \frac{C_c^2 k_B(T_2 - T_1)}{(C_1C_c + C_2C_c + C_1C_2)[(C_1 + C_c)R_1 + (C_2 + C_c)R_2]}$ is the average heat flow from the heat reservoir T_2 to T_1 [20]. Note that the seemingly large fraction of deviation in $\langle \Delta S^{(1)}_{\rm traj}\rangle$ can be comprehended by knowing that the average values of $\Delta S^{(1)}_{\rm traj}$ and $\Delta S^{(1)}_Q$ are much smaller than their standard deviations, the latter ranging in the order of k_B. Figure 3(c) exhibits the joint probability $\log P(\Delta S^{(1)}_Q, \Delta S^{(1)}_{\rm traj})$. The remarkable correlation (with a correlation coefficient 0.92) suggests the equivalence of $\Delta S^{(n)}_Q$ and $\Delta S^{(n)}_{\rm traj}$ in temperature-driven NESS.

IV. EFFECTS OF COARSE GRAINING IN CONFIGURATION SPACE AND TIME RESOLUTION

A. Coarse graining in configuration space

First we inspect the effects of coarse graining in configuration space. Naïvely speaking, a finer choice of $V_{\rm bin}$ should give better results, as stochastic trajectories can be described with more detail. On the other hand, in the derivation of $\Delta S^{(n)}_{\rm traj}$, occurrences of reverse trajectories are required. In particular, for trajectories with large positive entropy production, their reverse partners can be quite rare. Reducing $V_{\rm bin}$ differentiates similar trajectories into different trajectory types, and each trajectory category gets few events for finite sample size. As a result large fluctuations in $\Delta S^{(n)}_{\rm traj}$ may occur due to poor statistics. The problem gets even more severe when the system is driven far from equilibrium, where most trajectories have positive entropy production.

In this work the coarse-graining effect is explored using the current-driven single RC circuit for the case of $n = 4$. We first list the probability distributions $P(\Delta S^{(4)}_{\rm traj})$, $P(\Delta S^{(4)}_Q)$, and $P(\Delta S^{(4)}_{Q0})$ in Fig. 4(a) using $V_{\rm bin} = 1$ μV. The three distributions are quantitatively very much alike in the section of small entropy production. Furthermore, in most part of large positive entropy production, $P(\Delta S^{(4)}_{\rm traj})$ stays closer with $P(\Delta S^{(4)}_Q)$, as both distributions are lower than the primitive distribution $P(\Delta S^{(4)}_{Q0})$. The deviations are attributed to that $P(\Delta S^{(4)}_{\rm traj})$ and $P(\Delta S^{(4)}_Q)$ are derived from the set of trajectories in which the trajectories whose reverse counterparts cannot be found are discarded.

Figure 4(b) shows the number of discarded events (out of 10^6 total events in the original set of trajectories) and cross-correlation coefficient between $\Delta S^{(4)}_{\rm traj}$ and $\Delta S^{(4)}_Q$. The result indicates that as $V_{\rm bin}$ increases, the number of discarded events diminishes, and $\Delta S^{(4)}_{\rm traj}$ and $\Delta S^{(4)}_Q$ coincide. The average entropy production is presented in Fig. 4(c). Note that $\langle \Delta S^{(4)}_{Q0}\rangle$ is rather independent of $V_{\rm bin}$ and can represent the authentic entropy production. The strong correlation between $\Delta S^{(4)}_Q$ and $\Delta S^{(4)}_{\rm traj}$ is again demonstrated in their averages, while deviations from $\langle \Delta S^{(4)}_{Q0}\rangle$ emerge at finer values of $V_{\rm bin}$. Note that as $V_{\rm bin}$ further increases and approaches the standard deviation of $P_{\rm ss}(V)$, most trajectories are classified into very few categories, resulting in poor differentiation. Therefore, a proper choice of $V_{\rm bin}$ should satisfy a lower bound criterion to prevent poor statistics for finite sample size, and an upper bound criterion to ensure the capability of resolving state differences within the intrinsic fluctuations of the system.

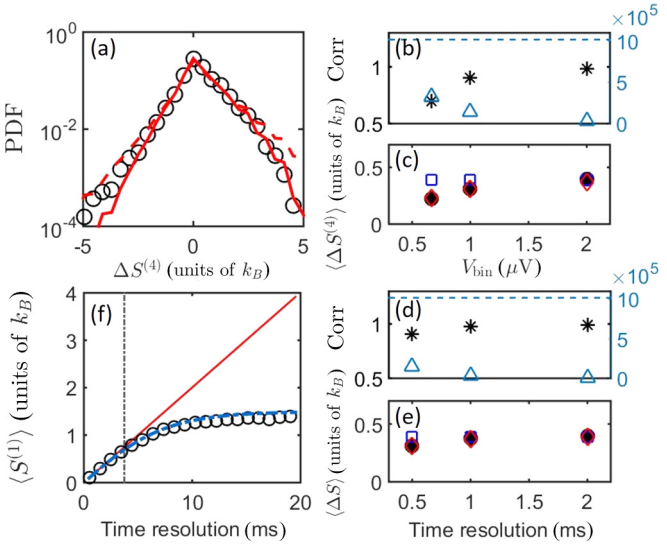

FIG. 4. Comparison of evaluation of entropy production using various configurational and temporal resolutions in current-driven NESS. (a) Probability distributions of $\Delta S^{(4)}_{\rm traj}$ (black circle), $\Delta S^{(4)}_{Q}$ (solid red line), and $\Delta S^{(4)}_{Q0}$ (dashed red line) using $V_{\rm bin} = 1$ μV. (b) Number of discarded events (blue triangle) and cross correlation between $\Delta S^{(4)}_{\rm traj}$ and $\Delta S^{(4)}_{Q}$ (black star) against $V_{\rm bin}$. The total number of events is 10^6 (indicated by the dashed line). (c) Average entropy production of $\Delta S^{(4)}_{\rm traj}$ (black solid circle), $\Delta S^{(4)}_{Q}$ (red diamond), and $\Delta S^{(4)}_{Q0}$ (blue square) for various chosen $V_{\rm bin}$. Panels (d) and (e): Similar analysis for sampling temporal resolutions Δt, $2\Delta t$, and $4\Delta t$, for trajectories of overall duration $\tau = 4\Delta t$ [the same symbols as panels (b) and (c); $V_{\rm bin} = 1$ μV is used]. (f) Average entropy production of single-time-step trajectories, $\langle \Delta S^{(1)}\rangle$, for various sampling temporal resolutions. Experimental results of $\Delta S^{(1)}_{\rm traj}$ (black circle) and $\Delta S^{(1)}_{Q}$ (red line), and theoretical prediction of $\Delta S^{(1)}_{\rm traj}$ (blue dashed line) are shown for comparison. The gray vertical dot-dashed line indicates the RC time constant of the circuit.

B. Effects of temporal resolution—fixed trajectory duration

As to the study of temporal resolution, we analyze trajectories of overall duration $\tau = 4\Delta t = 1.95$ ms using three different numbers of time steps: $n = 1$, 2, and 4. Thus the corresponding temporal resolutions are $4\Delta t$, $2\Delta t$, and Δt, respectively. A rougher temporal resolution means more skipped information. However, from our observation it does not seem to affect much on the determination of entropy production, as is shown in Figs. 4(d) and 4(e). Similar to the effects of coarse graining in configuration space, we find that with the use of a finer temporal resolution, the number of discarded events increases, and the average entropy production drops down slightly. This is again due to many large-ΔS events whose reverse counterparts can hardly be found are discarded.

The above observation indicates that a rougher temporal resolution does not affect the entropy production. However, this statement will fail if the temporal resolution is larger than the circuit relaxation time RC, the latter being approximately 4 ms in our setup. In such a regime, only the state changes over the time scale of autocorrelation of the system will be recorded in the calculation of trajectory entropy production. This will be further explained in the following subsection with the aid of theoretical analysis.

C. Effects of temporal resolution—single-time-step transition

In this subsection we study the effect of temporal resolution for the driven single RC circuit from a theoretical perspective. For simplicity, we focus on single-time-step trajectories only. The infinitesimal forward transition probability can be written down as [19]

$$P_F[V(dt)|V(0)] \sim \exp\left[\frac{-(M\dot{V}' + V')^2 dt}{2\Gamma}\right],$$

where $M \equiv RC$, $V' \equiv V - IR$, and $\Gamma \equiv 2Rk_BT$, and the symbol $\sim$ denotes equivalence up to a constant that remains invariant over time inversion. The finite-time forward transition probability can be evaluated via the path integral

$$P_F[V(\tau)|V(0)] \sim \int \mathcal{D}V(t) \exp\left[\frac{-\int (M\dot{V}' + V')^2 dt}{2\Gamma}\right] \sim \exp\left[\frac{-\int (M\dot{V}'_{op} + V'_{op})^2 dt}{2\Gamma}\right]. \quad (2)$$

The optimal path $V'_{op}(t)$ can be derived via the variational method: Defining the Lagrangian $L \equiv (M\dot{V}' + V')^2$, the optimal path suffices the condition $\delta \int L\, dt = 0$, and hence $\frac{d}{dt}(\frac{\partial L}{\partial \dot{V}'}) - \frac{\partial L}{\partial V'} = 0$. It leads to the equation $M\ddot{V}'_{op} = V'_{op}$. By straightforward evaluation one then gets

$$P_F[V(\tau)|V(0)] \sim \exp\left\{-\frac{M[V'(\tau)e^{M^{-1}\tau} - V'(0)]^2}{\Gamma(e^{2M^{-1}\tau} - 1)}\right\}. \quad (3)$$

The backward transition probability is simply derived by inverting the roles of $V(0)$ and $V(\tau)$ and replacing V' with $V'' \equiv V + IR$. Thus we have

$$\frac{\Delta S^{(1)}_{\rm traj}}{k_B} = \ln\frac{P_F}{P_R} = -\frac{M}{\Gamma}[V^2(\tau) - V^2(0)] + \frac{2MIR[V(0) + V(\tau)]}{\Gamma}\frac{e^{M^{-1}\tau} - 1}{e^{M^{-1}\tau} + 1}. \quad (4)$$

In the small-τ regime, the right-hand side of Eq. (4) approaches $\tau[V(\tau) + V(0)][I - C\dot{V}]/(2k_BT)$, and is thus equivalent to $\Delta S_Q/k_B$. However, the deviation from $\Delta S_Q/k_B$ grows up as τ approaches the system autocorrelation time RC. In the case $\tau \gg RC$, the total entropy evaluated by this means approaches the expression $RCI[V(0) + V(\tau)]/T$, the average entropy production over duration $2RC$. Figure 4(f) shows single-time-step entropy production average $\langle \Delta S^{(1)}\rangle$ for various trajectory duration τ (in this case τ equals time resolution), and $\langle \Delta S^{(1)}_{\rm traj}\rangle$ from experimental analysis (black circle) matches the theoretical prediction of Eq. (4) (blue line) very well. While $\langle \Delta S^{(1)}_{\rm traj}\rangle$ grows linearly with τ in the small-τ regime, it saturates at $2I^2R^2C/T \sim 1.5k_B$ and cannot properly stand for the correct entropy production when $\tau \gg RC$. On the contrary, $\langle \Delta S^{(1)}_{Q}\rangle$ (red line) truly represents the average entropy production of the system, as shown by its linear behavior over all values of τ. Therefore, similar to the discussion for $V_{\rm bin}$, an appropriate choice of temporal resolution should lie within some intermediate regime to prevent poor statistics and to ensure the capability of resolving state changes within the intrinsic autocorrelation time scale of the system.

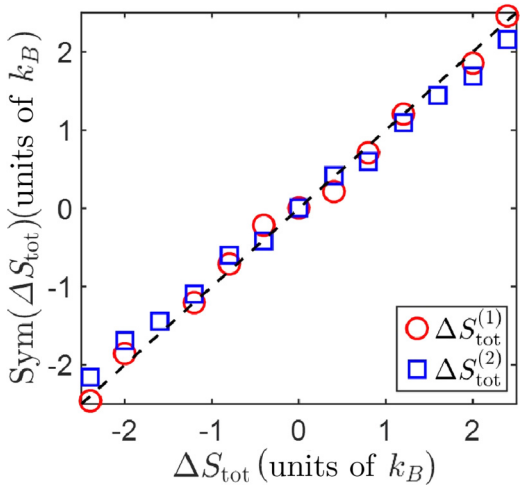

FIG. 5. Symmetry functions of total entropy production for $n = 1$ (red circle) and 2 (blue square) for the single *RC* circuit. $V_{\rm bin} = 1\ \mu$V is applied in the data analysis. A dashed black line of unit slope is provided as a guidance.

V. TEST OF FLUCTUATION THEOREM

In *RC* circuits, FT is often manifested through the consideration of the total entropy production $\Delta S_{\rm tot} = \Delta S_{\rm Sh} + \Delta S_Q$, where $\Delta S_{\rm Sh} = -k_B \ln \frac{P_{\rm ss}[V(t+\tau)]}{P_{\rm ss}[V(t)]}$ is the change in Shannon entropy, and ΔS_Q represents the heat entropy dissipation [22]. In this work, instead, we replace ΔS_Q by the trajectory entropy $\Delta S_{\rm traj}$. FT is examined through the consideration of a symmetry function [20,22] $\mathrm{Sym}(\Delta S_{\rm tot}) \equiv k_B \ln \frac{P(\Delta S_{\rm tot})}{P(-\Delta S_{\rm tot})}$, in which $P(\Delta S_{\rm tot})$ is the probability distribution of $\Delta S_{\rm tot}$. Figure 5 shows $\mathrm{Sym}(\Delta S^{(n)}_{\rm tot})$ for $n = 1$ and 2 for the case of current-driven single *RC* circuit. The validity of FT is demonstrated via the linear relation with unit slope. Note that, for this demonstration, the evaluation of $\Delta S_{\rm tot}$ relies on probability distributions only and requires no circuit parameter. Therefore, a fully probabilistic description of entropy production can be naturally envisioned.

VI. SUMMARY

In this work we experimentally demonstrate the equivalence between $\Delta S_{\rm traj}$ and ΔS_Q using two scenes of NESS, where the electric circuits are driven out of thermal equilibrium by a constant current source and temperature gradient, respectively. Trajectories with negative entropy production can be observed in these systems due to the broad distributions of entropy production. For the derivation of $\Delta S_{\rm traj}$ from experimental trajectories, one has to carefully choose the configuration and temporal resolutions in order to properly describe trajectories, while good statistics can still be achieved for determining transition probabilities. This equivalence is reaffirmed in the verification of FT with the trajectory entropy replacing its corresponding heat dissipation. Note that our data analysis is performed without the knowledge of circuit parameters, and thus this work serves as an experimental example where entropy production can be fully derived from a probabilistic description.

ACKNOWLEDGMENTS

The authors wish to thank Prof. Jae Dong Noh for fruitful discussions. This work has been supported by Ministry of Science and Technology in Taiwan under grant MOST 104-2112-M-008-003-MY3, 105-2112-M-008-019-MY2, and 105-2112-M-008-023. C.-L.L. acknowledges the support from NCTS thematic group Complex Systems.

APPENDIX A: EXPERIMENTAL DETAILS

The experimental setups in our studies are similar to two pioneer works [9,20]. The measured *RC* circuits in a metal shielding box is placed in a Faraday cage on an optical table. In the current-driven single *RC* circuit experiment, the constant current is generated by a battery in series with a 10-GΩ resistor. Its source resistance is therefore 10 GΩ and its thermal noise is 1000 times weaker than the studied systems. As for the coupled *RC* circuits connected to two different temperature baths, the resistor R_1 in a metal shielding box is cooled in a semiclosed liquid nitrogen dewar by liquid nitrogen vapor.

We use two-stage voltage amplifiers with gain of 10^4 to magnify the thermal voltages before sampling. The first stage with voltage gain of 100 is provided by Stanford Research Systems SIM910 or SR560 JFET amplifier. The second stage with gain of 100 is provided by the preamplifier in Stanford Research Systems SR780 spectrum analyzer. The amplified signals are filtered by a 160-kHz antialiasing filter, digitized

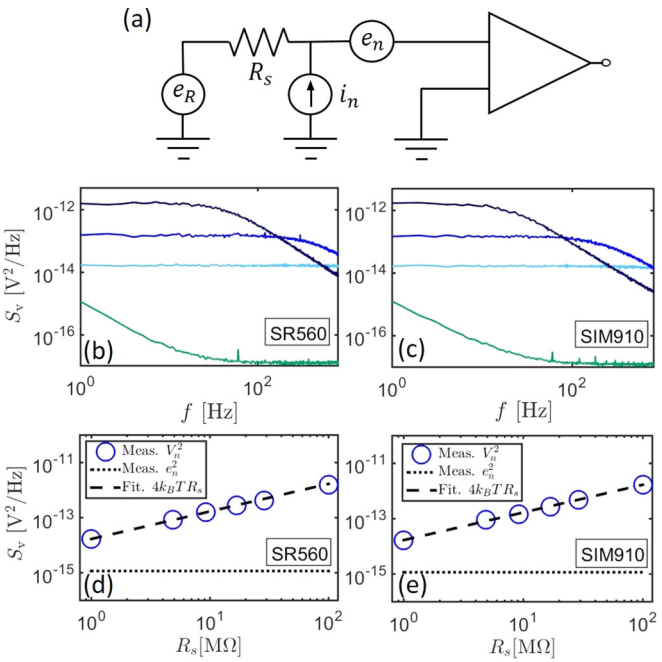

FIG. 6. Noise characterizations of voltage amplifiers SR560 and SIM910. (a) Amplifier noise model. Panels (b) and (c): Measured noise spectral density v_n^2 vs f for different R_s (0, 0.997, 9.20, and 100 MΩ, from bottom to top curves) for SR560 and SIM910, respectively. Panels (d) and (e): v_n^2 (at 1 Hz) vs R_s of SR560 and SIM910, respectively. The fitting result of e_R^2 against R_s is indicated as a dashed line, while the contribution of e_n^2 is plotted as a dotted line. The fitting parameters are listed in Table 1.

TABLE I. Noise model fitting parameters of voltage amplifiers.

Amplifier	i_n^2 [A^2/Hz]	$4k_BT$ [J]	e_n^2 [V^2/Hz] (measured)
SR560	-1.51×10^{-29}	1.68×10^{-20}	1.15×10^{-15}
SIM910	3.55×10^{-30}	1.67×10^{-20}	1.26×10^{-15}

at 262.1 kHz, and averaged over 128 digitized points for a sample to achieve sampling rate of 2048 Hz.

APPENDIX B: INPUT NOISE OF AMPLIFIERS

The input voltage noise e_n and input current noise i_n of both first stage amplifiers are characterized by measuring the noise spectral density v_n^2 against the source resistance R_s. According to the noise model of the voltage amplifier with a source resistance R_s at the input [see Fig. 6(a)] [23], three uncorrelated noises contribute to the overall input noise spectral density $v_n^2 = e_n^2 + i_n^2R_s^2 + 4k_BTR_s$, where $e_R^2 = 4k_BTR_s$ is the spectral density of the Johnson noise of R_s (also representing the studied noise signal), and $e_a^2 = e_n^2 + i_n^2R_s^2$ is the added noise spectral density by the amplifier. Figures 6(b) and 6(c) show the measured v_n^2 vs frequency f for different R_s (0, 0.997, 9.20, and 100 MΩ, from bottom to top curves) for SR560 and SIM910, respectively. The high-frequency roll-offs for large R_s due to the amplifier input capacitance (about tens of pF) are in evidence. The measured v_n^2 at low frequencies increases with R_s for both amplifiers. Figures 6(d) and 6(e) show v_n^2 (at 1 Hz) vs R_s of SR560 and SIM910, respectively. The measured v_n^2 increases linearly with R_s: No sign of quadratic dependence on R_s is observed. e_n^2 of the order of 10^{-15} V^2/Hz is directly determined by v_n^2 at $R_s = 0$. The data are fitted to the noise model to determine i_n^2 and T. The fitting gives insignificant i_n^2 and $T \simeq 300$ K for both amplifiers (see Table I). The fitting result of thermal noise power $4k_BTR_s$ is indicated as a dashed line, while the contributions of e_n^2 are plotted as a dotted line. For R_s of around 10 MΩ in our study, the contribution of e_a^2 (10^{-15} V^2/Hz, mainly from e_n) to v_n^2 (10^{-13} V^2/Hz) is indeed negligible.

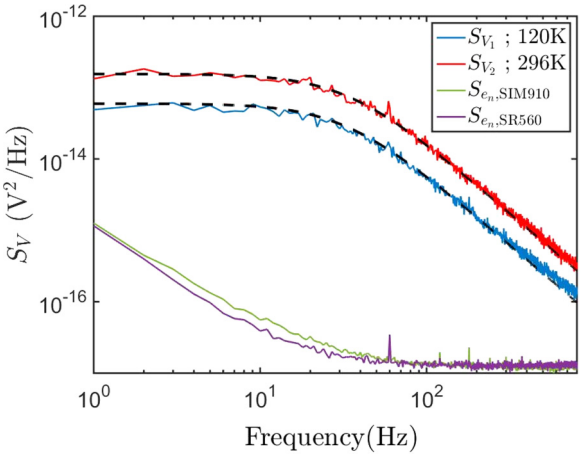

FIG. 7. The spectra of the measured thermal voltages of the studied circuit (red and blue solid lines) are compared to the input voltage noise spectra e_n^2 of SR560 and SIM910 (green and purple solid lines). The fitting to FDT (black dashed lines) gives the circuit parameters $C_1 = 488$ pF, $R_1 = 9.01$ MΩ, $T_1 = 120$ K, $C_2 = 420$ pF, $R_2 = 9.51$ MΩ, $T_2 = 296$ K, and $C_c = 100$ pF.

APPENDIX C: THERMAL NOISE OF STUDIED CIRCUIT

The measured thermal noise powers of coupled RC circuit [see Fig. 1(b) in the main text] with $C_c = 100$ pF are plotted (red and blue solid lines) in Fig. 7. The input voltage noise spectra e_n^2 of SR560 and SIM910 are shown (green and purple solid lines) for comparison. The thermal noise of the studied circuit overwhelms the added noise of the amplifiers by orders of magnitude. The circuit parameters are determined by fitting the measured noise powers to the fluctuation-dissipation theorem (FDT) [9,20]. The noise powers evaluated by FDT and the fitting parameters (black dashed lines in Fig. 7) match the measured noise powers perfectly. The FDT determined values are consistent with the nominal values of elements and the temperatures read by thermometry.

[1] G. M. Wang, E. M. Sevick, E. Mittag, D. J. Searles, and D. J. Evans, Phys. Rev. Lett. **89**, 050601 (2002).
[2] J. Liphardt *et al.*, Science **296**, 1832 (2002).
[3] D. J. Evans, E. G. D. Cohen, and G. P. Morriss, Phys. Rev. Lett. **71**, 2401 (1993).
[4] J. L. Lebowitz and H. Spohn, J. Stat. Phys. **95**, 333 (1999).
[5] G. E. Crooks, Phys. Rev. E **60**, 2721 (1999).
[6] C. Jarzynski, J. Stat. Phys. **98**, 77 (2000).
[7] D. M. Carberry, J. C. Reid, G. M. Wang, E. M. Sevick, D. J. Searles, and D. J. Evans, Phys. Rev. Lett. **92**, 140601 (2004).
[8] D. Collin *et al.*, Nature (London) **437**, 231 (2005).
[9] N. Garnier and S. Ciliberto, Phys. Rev. E **71**, 060101(R) (2005).
[10] S. Joubaud, N. B. Garnier, and S. Ciliberto, J. Stat. Mech. (2007) P09018.
[11] U. Seifert, Phys. Rev. Lett. **95**, 040602 (2005).
[12] R. Kawai, J. M. R. Parrondo, and C. Van den Broeck, Phys. Rev. Lett. **98**, 080602 (2007).
[13] U. Seifert, Rep. Prog. Phys. **75**, 126001 (2012).
[14] D. Andrieux, P. Gaspard, S. Ciliberto, N. Garnier, S. Joubaud, and A. Petrosyan, Phys. Rev. Lett. **98**, 150601 (2007).
[15] D. Andrieux *et al.*, J. Stat. Mech. (2008) P01002.
[16] F. Reif, *Fundamentals of Statistical and Thermal Physics* (McGraw-Hill, New York, 1965).
[17] R. van Zon, S. Ciliberto, and E. G. D. Cohen, Phys. Rev. Lett. **92**, 130601 (2004).
[18] K.-H. Chiang *et al.*, Europhys. Lett. **113**, 30001 (2016).
[19] K.-H. Chiang *et al.*, arXiv:1601.04776 (2016).
[20] S. Ciliberto, A. Imparato, A. Naert, and M. Tanase, Phys. Rev. Lett. **110**, 180601 (2013).
[21] G. B. Cuetara, M. Esposito, and A. Imparato, Phys. Rev. E **89**, 052119 (2014).
[22] S. Joubaud, N. B. Garnier, and S. Ciliberto, Europhys. Lett. **82**, 30007 (2008).
[23] P. Horowitz and W. Hill, *The Art of Electronics*, 3rd ed. (Cambridge University Press, New York, 2015).